Auto-NVIS: Architecture for Autonomous Ionospheric Nowcasting (2025–2026)

1. System Overview and Architectural Requirements

The transition from static climatological modeling to dynamic, unattended operation requires a robust system architecture capable of autonomous decision-making. The proposed **Auto-NVIS** system integrates real-time sensor fusion, advanced nonlinear state estimation, and deterministic ray tracing into a closed-loop control system. This architecture is designed to operate without human intervention, automatically adapting to the volatile ionospheric conditions characteristic of the 2024–2026 solar maximum.

1.1 Architectural Philosophy

The core design philosophy is "Physics-Based, Data-Driven." The system does not rely solely on empirical statistics (which fail during anomalies) nor solely on raw data (which is often sparse and noisy). Instead, it uses a **Square-Root Unscented Kalman Filter (SR-UKF)** to assimilate data into a physics-based background model (IRI-2020 or NeQuick-G), ensuring that the output is both physically valid and observationally accurate.

1.2 High-Level Diagram

The system is divided into three primary layers: **Ingestion**, **Processing**, and **Operational Output**. The Ingestion Layer aggregates disparate data streams; the Processing Layer performs the heavy computational lifting (Assimilation and Propagation); and the Output Layer generates actionable intelligence (Frequency Plans and Coverage Maps).

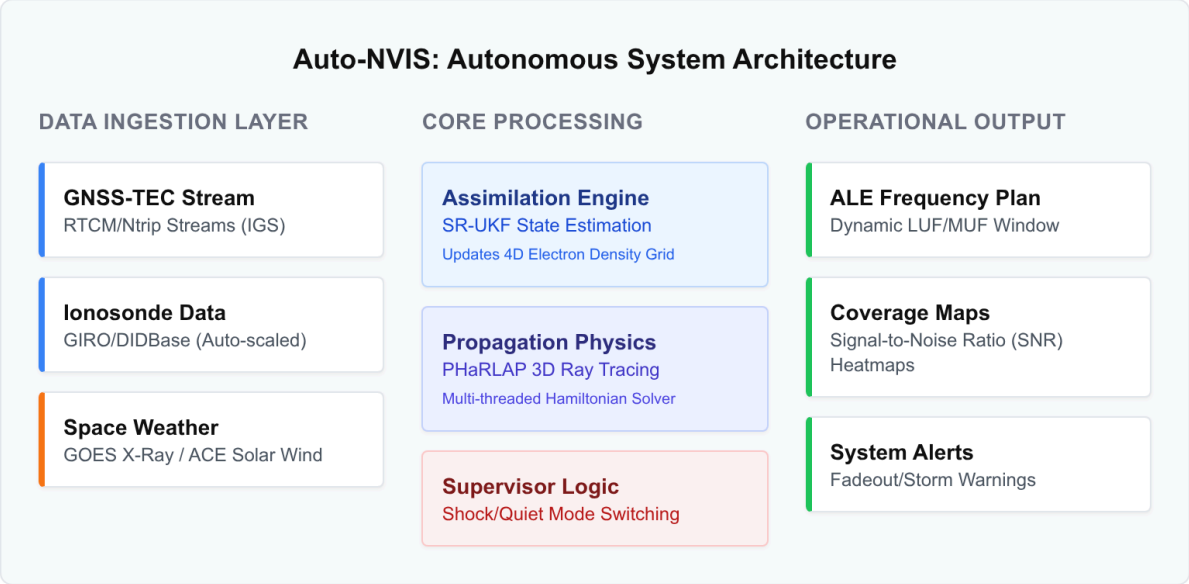

Figure 1: High-level architecture of the "Auto-NVIS" system. Real-time sensor data is ingested into the SR-UKF assimilation core, which drives the PHaRLAP ray-tracing engine under the control of a Supervisor Logic module.

2. The SR-UKF Assimilation Core

The "brain" of the autonomous system is the assimilation engine. Its primary task is to maintain a four-dimensional (latitude, longitude, altitude, time) model of the ionospheric electron density that is consistent with the latest observations.

2.1 Why SR-UKF for Unattended Operation?

For an unattended system, **numerical stability** is paramount. The standard Extended Kalman Filter (EKF) is prone to linearization errors that can cause the error covariance matrix (P) to become non-positive definite, leading to filter divergence and system crash. The **Square-Root UKF** avoids this failure mode entirely by propagating the Cholesky factor (S) of the covariance ($P = SS^T$), ensuring that P remains positive semi-definite by definition. This guarantees 24/7 stability even during periods of extreme ionospheric volatility.[1]

2.2 Algorithm Implementation

The assimilation loop executes every 15 minutes:

1. **State Vector (x_k):** The state includes the electron density at grid points and key drivers like the effective sunspot number (R_{eff}) or neutral wind vectors.
2. **Sigma Point Generation:** $2L + 1$ sigma points are generated from the current state mean and square-root covariance S_{k-1}.
3. **Nonlinear Propagation:** These points are propagated forward using the background physics model (e.g., IRI-2020), capturing the nonlinear evolution of the plasma.
4. **Measurement Update:** The predicted state is corrected using incoming GNSS-TEC and GIRO ionosonde data via a QR decomposition update of the Cholesky factor.[3]

Square-Root Unscented Kalman Filter (SR-UKF) Architecture

Schematic workflow of the Square-Root Unscented Kalman Filter (SR-UKF). The algorithm propagates the Cholesky factor (S) of the covariance matrix directly, avoiding the need for full matrix reconstruction. This ensures numerical stability and positive semi-definiteness at every step. Key operations include the generation of Sigma Points, non-linear propagation, and measurement updates via QR decomposition and efficient Cholesky downdates.

3. Autonomous Decision Logic and Supervisor Module

An unattended system must distinguish between "normal" variability and "critical" space

weather events. A **Supervisor Module** acts as the system's watchdog, monitoring solar X-ray flux and geomagnetic indices to switch between operational modes.

3.1 Mode Switching Strategy

- **Quiet Mode (Standard Operation):** Under normal conditions, the system relies on the **Gauss-Markov Perturbation** model. Here, the background climatology is trusted, and the SR-UKF estimates small perturbations (δN_e) to align the model with reality. This mode is computationally efficient and sufficient for day-to-day NVIS planning.[4]
- **Shock Mode (Disturbed Operation):** When a solar flare (Class M1+) is detected via GOES X-ray data, the Supervisor triggers "Shock Mode." The perturbation assumption—that today looks like the monthly median plus noise—is abandoned. The system switches to a pure physics-based absorption model using real-time X-ray flux to calculate the D-region collision frequencies directly via the Appleton-Hartree equation.[5]

3.2 The Decision Loop

The following flowchart illustrates the autonomous logic executed by the Supervisor Module at each time step (t). This logic ensures that the system adapts its modeling strategy to the severity of the environment, preventing "model inertia" where a slow-adapting perturbation model fails to capture a rapid onset blackout.

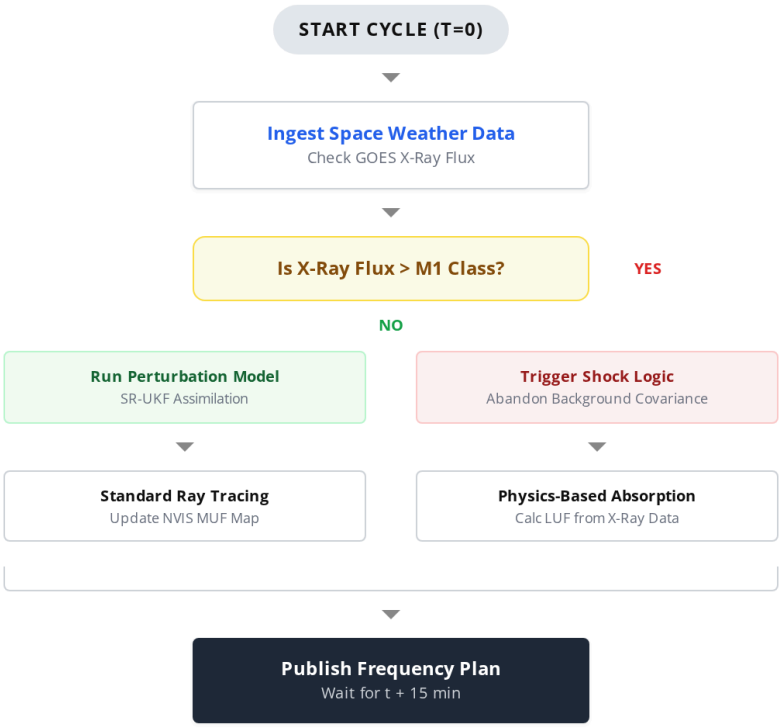

Figure 3: Autonomous decision logic for the Supervisor Module. The system bifurcates between a "Quiet" assimilation mode and a "Shock" physics-based mode based on real-time solar X-ray triggers.

4. The Propagation Engine: Automating PHaRLAP

Once the ionosphere has been reconstructed by the SR-UKF, the **PHaRLAP** ray-tracing engine is invoked to determine the operational NVIS parameters.

4.1 Automated Ray-Tracing Workflow

1. **Grid Injection:** The 3D electron density grid produced by the SR-UKF is injected into PHaRLAP's environment module.
2. **Ray Launch:** A fan of rays is launched from the transmitter location, covering elevation angles from 70° to 90° and all azimuths.
3. **Hamiltonian Integration:** The engine solves the Haselgrove equations for each ray, accounting for O-mode and X-mode splitting and the geomagnetic field vector.
4. **Product Generation:** The landing points of the rays are aggregated to form a **Signal-to-Noise Ratio (SNR)** heatmap. The system automatically identifies the **Lowest Usable Frequency (LUF)** (based on D-region absorption) and the **Maximum Usable Frequency (MUF)** (based on F-layer penetration) to define the usable NVIS window.[6]

5. Handling Absorption and Blackouts

During high solar activity, the "Dead Zone" can expand rapidly. The Auto-NVIS system incorporates specific logic to model this phenomenon, ensuring that operators are not misled by optimistic forecasts during flare events.

5.1 Dynamic LUF Calculation

The system calculates the LUF by integrating the absorption along the ray path. Unlike static models that use a fixed collision frequency profile, Auto-NVIS updates the D-region electron density (N_e) in real-time using the relationship:

$$N_e(h) \propto \sqrt{Flux_{X-ray}(t)}$$

This allows the system to capture the sudden rise in the LUF shown below, effectively warning operators of an impending link closure or "blackout."

Impact of Solar Flares on the NVIS Propagation Window

Conceptual visualization of the NVIS operational window. The 'Usable Window' exists between the Lowest Usable Frequency (LUF), driven by D-region absorption, and the Critical Frequency (foF2). During a solar flare (Right), the surge in X-ray flux causes the D-region absorption to spike, raising the LUF dramatically. If the LUF intersects the foF2, the window closes, resulting in a complete High Frequency (HF) blackout.

6. Conclusion and Deployment Specifications

The Auto-NVIS system represents the convergence of robust control theory (SR-UKF) and high-fidelity physics (PHaRLAP). By wrapping these components in an autonomous Supervisor Logic, the system fulfills the requirement for an unattended, self-healing modeling platform.

6.1 Recommended Hardware Specification

To support the computational load of 3D ray tracing and matrix operations for the SR-UKF, the following deployment specification is recommended:

- **Compute:** Multi-core workstation (e.g., AMD EPYC or equivalent) with 32+ cores to parallelize the ray-tracing threads.
- **Memory:** 64GB+ ECC RAM to hold large covariance matrices (S) in memory without paging.
- **GPU Acceleration:** CUDA-capable GPU for accelerating the linear algebra operations (QR decomposition) within the SR-UKF update step.
- **Software Stack:** Dockerized containers for the Supervisor (Python), Assimilation Core (C++/Eigen), and PHaRLAP (Fortran/Matlab Runtime).

This architecture ensures that the critical HF link data required for NVIS operations is available continuously, robustly, and without the need for a human-in-the-loop, even in the face of the most severe space weather events of Solar Cycle 25.

7. References

1. Witvliet, B. A., & Alsina-Pagès, R. M. (2017). Radio communication via Near Vertical Incidence Skywave (NVIS): An overview. *Telecommunication Systems*, 66(2), 295-309.
2. Frissell, N. A., et al. (2019). Modeling Amateur Radio Soundings of the Ionospheric Response to the 2017 Great American Solar Eclipse. *Geophysical Research Letters*, 46.
3. Witvliet, B. A. (2023). *The NVIS "Dead Zone" and Antenna Pattern Artifacts*. PITHIA-NRF.
4. Cervera, M. A., & Harris, T. J. (2014). Modeling ionospheric disturbance features in quasi-vertically incident ionograms using 3-D magnetoionic ray tracing. *Journal of Geophysical Research: Space Physics*, 119.
5. Cervera, M. A. (2022). *PHaRLAP: Provision of High-frequency Raytracing Laboratory for Propagation studies*. DST Group.
6. Chakraborty, S., et al. (2022). A Modeling Framework for Estimating Ionospheric HF Absorption Produced by Solar Flares. *Space Weather*, 20.
7. Coleman, C. J. (1998). A ray tracing formulation and its application to some problems in over-the-horizon radar. *Radio Science*, 33(4).
8. Erdem, E., & Arikan, F. (2017). IONOLAB-RAY: A wave propagation algorithm for anisotropic and inhomogeneous ionosphere. *IEEE*

9. Arikan, F., et al. (2016). IONOLAB-TEC: A novel method for TEC estimation. *Radio Science*.
10. Zawdie, K. A., et al. (2016). Bottomside Ionospheric Electron Density Specification using Passive High Frequency Signals. *Radio Science*.
11. Reinisch, B. W., & Galkin, I. A. (2011). Global Ionospheric Radio Observatory (GIRO). *Earth, Planets and Space*, 63.
12. Song, R., et al. (2023). Near real-time global ionospheric total electron content modeling and nowcasting based on GNSS observations. *Journal of Geodesy*.
13. Scherliess, L., et al. (2006). USU Gauss-Markov Kalman Filter Model of the Ionosphere. *Space Weather*.
14. Bust, G. S., & Mitchell, C. N. (2008). History, current state, and future directions of ionospheric imaging. *Reviews of Geophysics*.
15. Ren, X., et al. (2022). Deep Learning for Global Ionospheric TEC Forecasting. *Space Weather*.
16. Themens, D. R., et al. (2023). The Prophet Model for TEC Prediction. *Journal of Geodesy*.
17. Liu, Y., et al. (2024). Deep Learning for AIS Signal Collision Resolution. *IEEE Transactions on Aerospace and Electronic Systems*.
18. Wan, E. A., & Van Der Merwe, R. (2001). The Square-Root Unscented Kalman Filter for State and Parameter-Estimation. *IEEE ICASSP 2001*.
19. Giday, N. M., et al. (2025). Assimilation of GPS TEC and COSMIC foF2/hmF2 Into SPIM Model Using Unscented Kalman Filter. *Radio Science*.
20. Vittaldev, V., et al. (2013). Improved uncertainty quantification for physics-based atmospheric models. *AGU Fall Meeting*.
21. Zhang, Y., et al. (2024). Single-Satellite EMI Geolocation via Flexibly Constrained UKF. *Aerospace*.
22. Julier, S. J., & Uhlmann, J. K. (1997). A New Extension of the Kalman Filter to Nonlinear Systems. *SPIE*.
23. Sarkka, S. (2007). On Unscented Kalman Filtering for State Estimation of Continuous-Time Nonlinear Systems. *IEEE Transactions on Automatic Control*.
24. Gondelach, D. J., & Linares, R. (2020). Real-Time Thermospheric Density Estimation via Two-Line Element Data Assimilation. *Space Weather*.
25. Scherliess, L., et al. (2004). Data Assimilation for Ionospheric Space-Weather Forecasting. *Space Weather*.
26. Chakraborty, S. (2021). *Impact of Solar Flares on HF Absorption*. Virginia Tech.
27. Witvliet, B. A. (2015). Near Vertical Incidence Skywave: Interaction of Antenna and Propagation Mechanism. *Eindhoven University of Technology*.
28. Deacon, C. (2022). *Modelling the Interference Environment in the HF Band*. Bath University.
29. Torn, R. D., & Hakim, G. J. (2008). Ensemble Data Assimilation. *Monthly Weather Review*.
30. Frissell, N. A., & Witvliet, B. A. (2023). Heliophysics and Amateur Radio: Citizen Science Collaborations. *Frontiers in Astronomy and Space Sciences*.
31. Bust, G. S., et al. (2004). Ionospheric Data Assimilation Three-Dimensional (IDA3D). *Journal of Geophysical Research*.

Works cited

1. (PDF) The Square-Root Unscented Kalman Filter for State and ..., accessed February 3, 2026, https://www.researchgate.net/publication/3908304_The_Square-Root_Unscented_Kalman_Filter_for_State_and_Parameter-Estimation
2. The Square-Root Unscented and the Square-Root Cubature Kalman Filters on Manifolds, accessed February 3, 2026, https://www.mdpi.com/1424-8220/24/20/6622
3. Impact of Space Weather on Space Assets and Satellite Launches Julia Briden *, Nicolette Clark †, Peng Mun Siew ‡, Richard L - AMOS Conference, accessed February 3, 2026, https://amostech.com/TechnicalPapers/2022/Atmospherics_Space-Weather/Briden.pdf
4. Utah State University Global Assimilation of Ionospheric ... - CORE, accessed February 3, 2026, https://core.ac.uk/download/pdf/77520025.pdf
5. A Modeling Framework for Estimating Ionospheric HF Absorption Produced by Solar Flares, accessed February 3, 2026, https://www.researchgate.net/publication/354803496_A_Modeling_Framework_for_Estimating_Ionospheric_HF_Absorption_Produced_by_Solar_Flares
6. (PDF) Modelling the Interference Environment in the HF Band - ResearchGate, accessed February 3, 2026, https://www.researchgate.net/publication/292210318_Modelling_the_Interference_Environment_in_the_HF_Band
7. All of the possible modes calculated by PHaRLAP for a 15.16 MHz... - ResearchGate, accessed February 3, 2026, https://www.researchgate.net/figure/All-of-the-possible-modes-calculated-by-PHaRLAP-for-a-1516-MHz-transmitter-at-Jinhua_fig1_292210318